Compressive Energy Detection for Blind Coarse Wideband Sensing: Comparative Performance Study

Anastasia Lavrenko and Reiner S. Thomä
Institute for Information Technology
Technische Universität Ilmenau
Helmholzplatz 2, 98693, Ilmenau, Germany
Email: {anastasia.lavrenko, reiner.thomae}@tu-ilmenau.de

Andreas Bollig
Institute for Theoretical Information Technology
RWTH Aachen University
Sommerfeldstr. 24, 52074, Aachen, Germany
Email: bollig@ti.rwth-aachen.de

***Abstract*—Wideband signal acquisition and spectrum sensing play a crucial role in a number of applications. In this work we discuss the task of blind spectrum sensing of frequency-sparse wideband signals sampled at sub-Nyquist rates. We show how in a generic sub-Nyquist sampling framework the results of the support recovery can be directly used for coarse multichannel energy detection. We numerically study the performance of the proposed compressive energy detector and compare it with that of the related approaches. Our results demonstrate that it outperforms its closest counterpart that operates on the recovered power spectral density and provides a comparable performance to the Nyquist-rate energy detector in the high SNRs.**

***Keywords*—wideband, spectrum sensing, sub-Nyquist, energy detection, support recovery**

I. Introduction

The task of acquiring a wide frequency band that is comprised of multiple communication sub-bands is crucial in a number of applications including cognitive radio (CR), spectrum monitoring and radio surveillance. Sampling rate required for traditional Nyquist sampling grows proportionally with the bandwith of interest making analog to digital conversion one of the main receiver' bottlenecks. However, it has been recently shown that by applying compressed sensing paradigm to the reception of wideband signals it becomes possible to significantly reduce sampling rates while preserving the signal information content, provided that the signal's energy occupies only a fraction of the total frequency band [1], [2], [3]. Given such a sub-Nyquist sampled signal the primary aim of wideband spectrum sensing is to detect which parts of its spectrum are occupied and which are not.

In a blind scenario when the positions and the bandwidths of the signal sub-bands are unknown in advance, one has to additionally solve an associated estimation problem. One way of dealing with it is to recover and analyze the edge spectrum, as proposed in [4] for instance. Another approach is to first recover the signal's spectrum from the compressed measurements, then split it into multiple narrowband channels and apply conventional signal detection methods, e.g., energy detection, in each of them [5], [6], [7], [8]. This can be done on either the frequency/power spectrum computed from a reconstructed Nyquist sampled signal equivalent or on the power spectral density (PSD) estimated directly from the compressed measurements as in [6], [8], and [9]. Note that in the blind scenario this will result in a coarse estimation of the spectrum occupancy since the positions and the bandwidths of these narrowband channels might not exactly coincide with those of the signal sub-bands. Finally, it was pointed out in [10] that the sub-Nyquist sampling framework already provides coarse spectrum sensing functionality at a resolution of the spectral channelization of the sampler.

Motivated by the latter approach, in this work we investigate energy based blind wideband sensing of sub-Nyquist sampled sparse multiband signals. We show that in a generic sub-Nyquist sampling framework one can coarsely detect the presence of the signal energy directly from the compressed measurements, i.e., without the need to perform full signal or PSD recovery. Taking advantage of the implicit spectral channelization that happens during the signal acquisition step, we apply sparse recovery in order to estimate average signal energy within the channalization sub-bands of the sampler from the observation covariance matrix. Due to the complex iterative nature of commonly used sparse solvers rigorous performance analysis of such a compressive energy detector does not seem to be feasible. Therefore we perform an extensive numerical study instead. For various signal scenarios we compare the empirical probabilities of correct detection, false alarm and missed detection of the proposed approach and those of the related approaches based on the multichannel energy detection. Our results suggest that the proposed direct coarse wideband sensing outperforms its counterpart that operates on the recovered power spectrum, provided that the sensing parameters are equal. An additional advantage comes from the fact that it can be used without setting an arbitrary detection threshold. It is worth noting that the spectral resolution of the proposed detector is dictated by the parameters of the sampling scheme and hence it is fixed. We demonstrate therefore how the spectral accuracy of the resulting occupancy estimate depends on the actual positions and bandwidths of the signal sub-bands and numerically investigate its influence on the overall detection performance.

II. Sub-Nyquist Sampling of Analog Sparse Multiband Signals

A. Multiband Signal Model

Consider a complex-valued continuous signal $s(t)$ bandlimited to $\mathcal{F}_{\mathrm{n}} = [0, W)$. Its energy is distributed over K disjoint frequency intervals of widths B_i and central frequencies f_{c_i}. The Fourier transform of $s(t)$ is given by

$$S(f) = \int_{-\infty}^{+\infty} s(t) e^{-\jmath 2\pi f t} \mathrm{d}t, f \in \mathcal{F}_{\mathrm{n}} \tag{1}$$

and the support of $S(f)$ is defined as

$$\mathcal{F} = \bigcup_{i=1}^{K} [f_{\mathrm{c}_i} - B_i/2, f_{\mathrm{c}_i} + B_i/2] \subset \mathcal{F}_{\mathrm{n}}. \quad (2)$$

This way in the absence of noise $S(f) \triangleq 0,\ f \notin \mathcal{F}$. Note that the complex-valued model was chosen for the sake of presentation simplicity only.

The signal's spectral support $\mathcal{F}$ is assumed to be arbitrary. The positions of the signal sub-bands that contain energy are unknown beforehand and individual signals within these sub-bands are independent from each other. Additionally, the total bandwidth W is supposed to be only sparsely occupied, meaning that the Lebesgue measure $\lambda(\mathcal{F}) = \sum_i B_i$ of the spectral support is $< 0.5W$ [1].

B. Sub-Nyquist Signal Acquisition

Suppose that the Nyquist range $\mathcal{F}_{\mathrm{n}} = [0, W)$ is virtually split into L consecutive non-overlapping blocks of width $f_{\mathrm{s}} = W/L$, so that $\mathcal{F}_{\mathrm{n}} = \bigcup_{\ell=1}^{L} \mathcal{F}^{\ell}$ with $\mathcal{F}^{\ell} = [(\ell-1)f_s, \ell f_s)$. The core idea behind Xampling [11] is to treat the original wideband signal $s(t)$ as a finite union of continuous bandpass spaces $\mathcal{F}^{\ell}$ where $S(f) = [S^{(1)}(f), S^{(2)}(f), \ldots, S^{(L)}(f)]$ and

$$S^{(\ell)}(f) = \begin{cases} S(f), & \text{if } f \in \mathcal{F}^{\ell} \\ 0, & \text{otherwise.} \end{cases} \quad (3)$$

By analog aliasing of the individual components $S^{(\ell)}(f)$ to the baseband one can reduce the effective signal bandwidth to be sampled from W to f_s. During this process the baseband portions of the original signal are additionally weighted and combined together. The presence of M such down-converters with different weighting coefficients ensure signal recoverability. Note that the resulting sampling rate per branch f_{s} has to be $\geq \max_i(B_i)$ [3], [10], [11].

Denote the output of such a sampler as $\boldsymbol{y}[n] = [y_1[n], y_2[n], \cdots, y_M[n]]^{\mathrm{T}}$ where $(\cdot)^{\mathrm{T}}$ is the vector transpose and M is the number of parallel down-converting branches. The process of sub-Nyquist sampling can be represented then in a matrix from as

$$\boldsymbol{y}[n] = \boldsymbol{A}\boldsymbol{z}[n], \quad (4)$$

where $\boldsymbol{z}[n] = [z_1[n], z_2[n], \cdots, z_L[n]]^{\mathrm{T}}$ and $z_\ell[n]$ is the time-series corresponding to the baseband version of the bandpass signal component $S^{(\ell)}(f)$. The $M \times L$ matrix $\boldsymbol{A}$ is a sensing matrix that weighs and linearly combines these together.

Applying the discrete-time Fourier transform (DTFT) to both sides of (4), we have that in the frequency domain

$$\dot{\boldsymbol{y}}(f) = \boldsymbol{A}\dot{\boldsymbol{z}}(f), f \in \mathcal{F}_{\mathrm{s}}, \quad (5)$$

where $\mathcal{F}_{\mathrm{s}} = [0, f_s)$, $\dot{\boldsymbol{y}}(f)$ is a vector containing the DTFTs of $\boldsymbol{y}[n]$, and $\dot{\boldsymbol{z}}(f)$ is an $L \times 1$ vector with elements given by

$$\dot{z}_\ell(f) = S^{(\ell)}(f + \ell f_s), f \in \mathcal{F}_{\mathrm{s}}. \quad (6)$$

Relations (4) and (5) link the spectrum of the digital low-rate output measurements $\boldsymbol{y}[n]$ to the unknown frequency support $\mathcal{F}$ of the analog input signal $s(t)$. The two most well known sampling schemes practically implementing (4) include Periodic Non-uniform Sampling (PNS) [1], [2] and the Modulated Wideband Converter (MWC) [3].

Once the signal $\boldsymbol{y}[n]$ is acquired the goal of wideband spectrum sensing is to detect which parts of the total band of interest W contain signal energy and which do not. To do so we propose to take advantage of the relations between $S(f)$, $\dot{\boldsymbol{z}}(f)$ and $\boldsymbol{y}[n]$ revealed by (4), (5) and (6) in order to directly detect the presence of the signal energy within the consequent spectral blocks $\mathcal{F}_\ell$ from $\boldsymbol{y}[n]$.

III. Direct Coarse Wideband Spectrum Sensing

A. Direct Compressive Energy Detector

Consider an observation covariance matrix $\boldsymbol{R}$ computed from the compressed measurements $\boldsymbol{y}[n]$ as

$$\boldsymbol{R} = \sum_{n=-\infty}^{\infty} \boldsymbol{y}[n]\boldsymbol{y}[n]^{\mathrm{H}} = \int_{f \in \mathcal{F}_{\mathrm{s}}} \dot{\boldsymbol{y}}(f)\dot{\boldsymbol{y}}(f)^{\mathrm{H}} \mathrm{d}f, \quad (7)$$

where $(\cdot)^{\mathrm{H}}$ stands for the Hermitian transpose. Substituting (5) into (7), we have

$$\boldsymbol{R} = \int_{f \in \mathcal{F}_{\mathrm{s}}} \boldsymbol{A}\dot{\boldsymbol{z}}(f)\dot{\boldsymbol{z}}(f)^{\mathrm{H}}\boldsymbol{A}^{\mathrm{H}} \mathrm{d}f = \boldsymbol{A}\boldsymbol{R}_{\mathrm{z}}\boldsymbol{A}^{\mathrm{H}}, \quad (8)$$

where $\boldsymbol{R}_{\mathrm{z}}$ is an $M \times M$ matrix. From (5) it is easy to see that the diagonal elements $(R_{\mathrm{z}})_{jj}$ of $\boldsymbol{R}_{\mathrm{z}}$ contain energy of the corresponding bandpass signal components so that

$$(R_{\mathrm{z}})_{jj} = \int_{f \in \mathcal{F}_{\mathrm{s}}} |\dot{\boldsymbol{z}}_j(f)|^2 \mathrm{d}f = \int_{f \in \mathcal{F}^j} |S^{(j)}(f)|^2 \mathrm{d}f, \quad (9)$$

where $j = 1, 2, \cdots, M$. The non-diagonal elements $(R_{\mathrm{z}})_{kj:k\neq j}$ therefore represent cross-correlation terms between the k^{th} and the j^{th} signal components. Hence, when the signals within the individual sub-bands are uncorrelated, $\boldsymbol{R}_{\mathrm{z}}$ becomes a diagonal matrix with $\tilde{K} \leq 2K$ non-zero elements on the main diagonal.

Using a well-known property of the Kroneker product for matrix vectorization, we can write

$$\boldsymbol{r} = \mathrm{vec}(\boldsymbol{R}) = (\boldsymbol{A}' \otimes \boldsymbol{A}) \cdot \boldsymbol{r}_{\mathrm{z}} = (\boldsymbol{A}' \odot \boldsymbol{A}) \cdot \mathrm{diag}(\boldsymbol{R}_{\mathrm{z}}), \quad (10)$$

where $\boldsymbol{r}_{\mathrm{z}} = \mathrm{vec}(\boldsymbol{R}_{\mathrm{z}})$ is a $\tilde{K}$-sparse $L^2 \times 1$ vector, $(\cdot)'$ is the matrix conjugation, $\otimes$ and $\odot$ denote the Kroneker and Khatri-Rao products, respectively [8]. Thus, given the measurements $\boldsymbol{y}[n]$, one can recover the unknown support $\mathcal{S}$ of $\boldsymbol{z}(f)$ by solving a typical sparse recovery problem of a following form

$$\hat{\mathcal{S}} = \mathrm{supp}\big(\arg\min_{\boldsymbol{d}_{\mathrm{z}}} (\|\boldsymbol{d}_{\mathrm{z}}\|_1)\big) \text{ s.t. } \boldsymbol{r} = \boldsymbol{A}^{\mathrm{KR}} \cdot \boldsymbol{d}_{\mathrm{z}}, \quad (11)$$

where $\boldsymbol{r} = \mathrm{vec}\big(\sum_{n=-\infty}^{\infty} \boldsymbol{y}[n]\boldsymbol{y}[n]^{\mathrm{H}}\big)$, $\boldsymbol{A}^{\mathrm{KR}} = (\boldsymbol{A}' \odot \boldsymbol{A})$, and $\boldsymbol{d}_{\mathrm{z}} = \mathrm{diag}(\boldsymbol{R}_{\mathrm{z}})$.

Now consider an $L \times 1$ binary occupancy vector $\boldsymbol{b}$, each element of which is given by

$$b_\ell = \begin{cases} 1, & \text{if } \int_{\mathcal{F}^\ell} |S^{(\ell)}(f)|^2 \mathrm{d}f > 0 \\ 0, & \text{otherwise} \end{cases}. \quad (12)$$

We have that $b_\ell = 0\ \forall \ell \notin \mathcal{S}$ and $\|\boldsymbol{b}\|_0 = |\mathcal{S}|$ where $\mathcal{S}$ contains the positions of the non-zero elements of $\boldsymbol{d}_{\mathrm{z}}$. Therefore, once the support $\mathcal{S}$ is estimated one can detect the presence of the signal energy in the ℓ-th spectral block $\mathcal{F}^\ell$ by applying one of the following decision rules:

1) Direct non-parametric decision rule (DDR): The support $\mathcal{S}$ contains the positions of the non-zero entries of $\mathrm{diag}(\boldsymbol{R}_{\mathrm{z}})$ which are identical to the positions of the non-zero elements in $\dot{\boldsymbol{z}}(f)$. The decision rule for signal detection is thus simply given by

$$b_\ell = \begin{cases} 1, & \text{if } \ell \in \hat{\mathcal{S}} \\ 0, & \text{otherwise} \end{cases}, \tag{13}$$

where $\hat{\mathcal{S}}$ is the recovered support.

2) Energy based decision rule (EDR): Given the estimate of the support $\hat{\mathcal{S}}$ and taking into account (10), the energy $\xi_\ell = \int_{\mathcal{F}^\ell} |S^{(\ell)}(f)|^2 \mathrm{d}f$ within each of the spectral block can be estimated as

$$\hat{\xi}_\ell = \begin{cases} \boldsymbol{\Psi}_\ell^\dagger \cdot \boldsymbol{r} & , \text{if } \ell \in \hat{\mathcal{S}} \\ 0 & , \text{otherwise} \end{cases}, \tag{14}$$

where $\boldsymbol{\Psi} = \boldsymbol{A}' \odot \boldsymbol{A}$, $\boldsymbol{\Psi}_n$ contains the n-th column of $\boldsymbol{\Psi}$ and $(\cdot)^\dagger$ denotes the Moore-Penrose pseudo-inverse. Hence, the following decision rule can be applied

$$b_\ell = \begin{cases} 1, & \text{if } \hat{\xi}_\ell > \zeta \\ 0, & \text{otherwise} \end{cases}, \tag{15}$$

where ζ is some threshold defined in advance. Note that (15) becomes (13) when $\zeta = 0$.

B. Coarse Spectral Occupancy Estimation

The detection results from (13) and (15) can be used to estimate coarse spectral support $\hat{\tilde{\mathcal{F}}}$ as follows

$$\hat{\tilde{\mathcal{F}}} = \bigcup_{\{\ell: b_\ell \neq 0\}} \mathcal{F}^\ell, \ \lambda(\hat{\tilde{\mathcal{F}}}) = \kappa f_{\mathrm{s}}, \tag{16}$$

where for DDR $\kappa = |\boldsymbol{b}| = |\hat{\mathcal{S}}|$ and for EDR $\kappa = |\boldsymbol{b}| \leq |\hat{\mathcal{S}}|$.

Suppose that the support $\mathcal{S}$ is estimated correctly. Then the difference between the true spectral support $\mathcal{F}$ and the estimated coarse spectral support $\hat{\tilde{\mathcal{F}}}$ is

$$0 \leq \delta_f = \lambda(\hat{\tilde{\mathcal{F}}}) - \lambda(\mathcal{F}) \leq 2K f_{\mathrm{s}}, \tag{17}$$

where the upper bound is due to the fact that a single signal sub-band can potentially contribute to up to two consequent spectral blocks $\mathcal{F}^\ell$. The actual value of δ_f depends on the current positions f_{c_i} and bandwidths B_i of the signal sub-bands: it achieves 0 in the case when $B_i = f_s$ and $f_{ci} = f_s/2 \ \forall i \in [1, K]$, whereas for any fixed values of B_i, it is lower bounded by $K f_{\mathrm{s}} - \sum\limits_i B_i$.

Figure 1 graphically demonstrates how the resulting spectral accuracy depends on the difference between the channelization and signal sub-band parameters for the case of a single signal sub-band. It shows that there are two distinct areas: triangular area around $f_{\mathrm{c}} = (2k+1)f_s/2, \ k \in \mathbb{Z}$ where the estimation error is upper-bounded by f_s (depicted by the light grey colors) and the area mostly concentrated around the edges of the sampler' channel where the error is greater or equal to f_s and upper-bounded by $2f_s$ (depicted by the dark grey colors). This indicates that for a uniformly distributed unknown support $\mathcal{F}$ with $B_i \simeq f_{\mathrm{s}}$, with a high probability each signal sub-band is split between two neighboring spectral blocks resulting both in the increase of the sparsity order of $\boldsymbol{r}_{\mathrm{z}}$ and decrease of the signal-to-noise ratio within the block. The degree to which this has an effect on the spectrum sensing performance will be investigated numerically in Section IV-C.

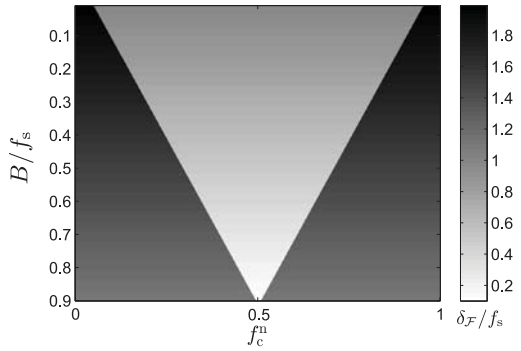

Fig. 1: Normalized difference $\delta_{\mathcal{F}}/f_{\mathrm{s}}$ vs. normalized signal sub-band position $f_{\mathrm{c}}^{\mathrm{n}} = f_{\mathrm{c}}/f_{\mathrm{s}} - \lfloor f_{\mathrm{c}}/f_{\mathrm{s}} \rfloor$ vs. normalized bandwidth B/f_{s} for the number of signal sub-bands $K = 1$, where $\lfloor \cdot \rfloor$ denotes the operation of rounding to the nearest smaller integer

IV. Numerical Study

A. Performance Metrics

Naturally, for each of the L spectral blocks $S^{(\ell)}(f)$ we can introduce probabilities of false alarm $P_{\mathrm{fa},\ell}$ and missed detection $P_{\mathrm{md},\ell}$ so that

$$P_{\mathrm{fa},\ell} \triangleq Pr(b_\ell = 1|_{\int_{\mathcal{F}^\ell} |S^\ell(f)|^2 \mathrm{d}f = 0}), \tag{18}$$

$$P_{\mathrm{md},\ell} \triangleq Pr(b_\ell = 0|_{\int_{\mathcal{F}^\ell} |S^\ell(f)|^2 \mathrm{d}f > 0}). \tag{19}$$

In order to evaluate the overall performance of the multichannel signal detection, we define cumulative performance metrics such as

- the total probability of correct detection P_d

$$P_d \triangleq Pr(b_\ell = 1 \, \forall \ell \in \mathcal{S}, \, b_k = 0 \, \forall k \in \mathcal{S}'), \tag{20}$$

  where $\mathcal{S}' = \{1, 2, \cdots, L\} \backslash \mathcal{S}$ and $\{\cdot\} \backslash \{\cdot\cdot\}$ denotes the relative complement of $\{\cdot\}$ in $\{\cdot\cdot\}$;
- the probability P_{fa} of at least one spectral block being falsely detected as occupied

$$P_{\mathrm{fa}} \triangleq Pr(\exists k \in \mathcal{S}' : \, b_k = 1); \tag{21}$$

- the probability P_{md} of at least one spectral block $S^\ell(f)$ being falsely detected as non-occupied

$$P_{\mathrm{md}} \triangleq Pr(\exists k \in \mathcal{S} : \, b_k = 0). \tag{22}$$

Derivation of general formulas linking (20)-(22) with (18)-(19) is non-trivial since they depend both on the signal properties and the recovery algorithm used to estimate $\hat{\mathcal{S}}$ in (11). Altogether, it makes the theoretical analysis of the problem at hand not feasible. Therefore we perform a numerical performance study instead.

B. Simulation Setup

In this section we present the results of a series of numerical simulations where the test multiband signals were generated in the frequency domain by representing the Nyquist range $\mathcal{F}_{\mathrm{n}} = [0, W)$ with a dense grid of LN equidistant points. Each test signal had exactly K occupied sub-bands of equal bandwidth B such that

$$S[f_k] = \begin{cases} \sigma_{\mathrm{s},i} \mathrm{e}^{\jmath\phi[f_k]} + w[f_k] & , f_k \in \bigcup\limits_{i=1}^{K} [a_i, b_i) \\ w[f_k] & , \text{otherwise} \end{cases}, \tag{23}$$

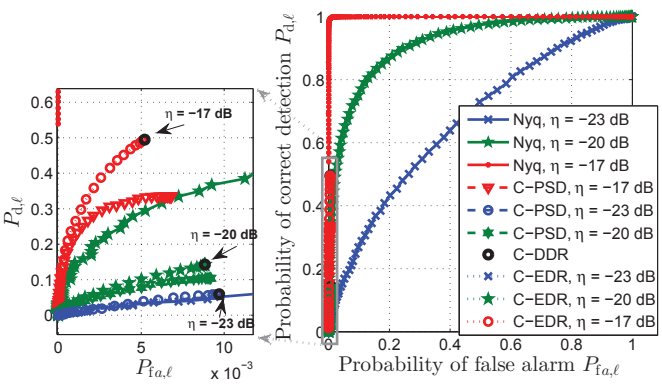

Fig. 2: Probability of correct detection per block $P_{\mathrm{d},\ell}$ vs. probability of false alarm per block $P_{\mathrm{fa},\ell}$ for the case of a single signal sub-band that occupies exactly one spectral block

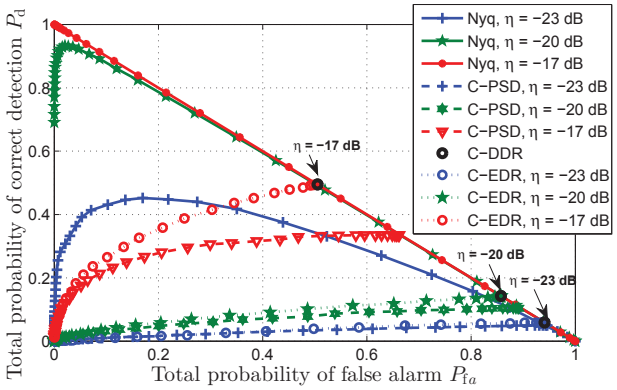

Fig. 3: Total probability of correct detection P_{d} vs. total probability false alarm P_{fa} for the case of a single signal sub-band that occupies exactly one spectral block

where $w[f_k]$ is additive wideband noise, $f_k = k\frac{W}{LN}$, $a_i = \langle f_{\mathrm{c}_i} - B/2\rangle$, $b_i = \langle f_{\mathrm{c}_i} + B/2\rangle$ and $\langle\cdot\rangle$ denotes the operation of rounding to the nearest grid point. Parameters $\phi[f_n]$, $\sigma_{\mathrm{s},i}$ and f_{c_i} were drawn independently from uniform distributions $\mathcal{U}(-\pi,\pi)$, $\mathcal{U}(0,1)$ and $\mathcal{U}(B/2, W-B/2)$, respectively. The signal powers $\sigma_{\mathrm{s},i}$ were normalized so that $\sum_{i=1}^{K}\sigma_{\mathrm{s},i}^2 = 1$. The noise $w[f_k]$ was modeled as an i.i.d$\sim$circularly symmetric complex Gaussian white noise with variance σ_0^2 where the total signal-to-noise ratio was defined as $\eta = 1/\sigma_0^2$. The sensing matrix $\boldsymbol{A}$ was chosen randomly with entries $a_{k,p}$ drawn independently from a complex normal distribution $\mathcal{CN}(0,1)$, after which they were normalized to an equal row norm, i.e., so that $\|\boldsymbol{a}_p\|_2 = 1$. The actual values of the parameters used throughout the simulations can be found in Table I.

C. Performance Study

We study the applicability of the compressive energy detector from III-A by comparing it with alternative multichannel signal detection methods based on the estimation of the signal's power spectral density. For the PSD estimation we used two approaches: direct reconstruction from $\boldsymbol{y}[n]$ as in [8] and square magnitude of the originally Nyquist-sampled signal $S[f_k]$. Note that we did not consider an approach for estimating PSD from the reconstructed Nyquist sampled signal equivalent since it has been already shown to provide slightly worse performance than the recovered PSD [8]. For the estimation of the support $\mathcal{S}$ in (11) we used the Orthogonal Matching Pursuit (OMP) from [12]. The number K of the active signal sub-bands was assumed to be known a priori and used as a stopping criteria for the OMP.

In order to perform a direct comparison, once the power spectrum was estimated, it was split into L non-overlapping consecutive blocks of bandwidth f_s, after which energy detection was performed independently for each of them. The considered algorithms are further referred to as: C-DDR for the proposed direct compressive energy detector with the direct decision rule from (13) and C-EDR for the proposed direct compressive energy detector with the energy based decision rule from (15), C-PSD for the energy detection on the recovered PSD, and Nyq for the energy detection on the Nyquist sampled signal.

1) Single signal sub-band: We begin by considering a single signal sub-band with a central frequency that is an odd multiple of $f_s/2$, meaning that it always occupies exactly one spectral block $S_\ell[f_k]$, i.e., $|\mathcal{S}| = K = 1$. Figure 2

TABLE I: Choice of Parameters for Simulations

Signal Parameters	Sampling Parameters
$K \in [1,3]$	$f_{\mathrm{NYQ}}/B = 105$
$B = 19$ MHz	$L = 97 \leq f_{\mathrm{NYQ}}/B$
$f_{\mathrm{NYQ}} = 2$ GHz	$f_{\mathrm{s}} \approx 20.6$ MHz
$N = 50$	$M = 30$

presents the receiver operating characteristic (ROC), i.e., posterior probability of detection versus posterior probability of false alarm, per spectral block. Note that since C-DDR does not require setting a threshold, it is represented by a single, black, dot for each SNR. This also results in the posterior probabilities of false alarm and correct detection not spanning the whole range of $[0,1]$ for both C-DDR and C-EDR. One can see that the reference Nyq scheme that corresponds to the Nyquist-rate sampling provides better performance than all three compressed detectors in the considered SNR range.

However, ROC curves for the total posterior probabilities of correct detection and false alarm presented on Figure 3 demonstrate already a slightly different trend. For the reference Nyquist-sampled scheme it is characterized by the inversion of the characteristic for high false alarm rates and overall deterioration of the performance with regard to the SNR. Contrarily, the character of the ROC curves for C-DDR, C-EDR and C-PSD is not significantly affected except for the scaling factor. This is because, when applying sparse recovery algorithms, the false detection can only occur when the support was already recovered wrongly. Thus for the OMP with the properly set stopping criteria $P_{\mathrm{fa}} \approx P_{\mathrm{fa},\ell} \cdot L$ and $P_{\mathrm{d}} = P_{\mathrm{md},\ell}$.

The resulting total posterior probability of correct detection P_{d} versus SNR depicted on Figure 4 demonstrates that the proposed C-DDR detector outperforms the compressive PSD estimator C-PSD in the whole SNR range, while its energy based modification C-EDR provides similar to C-PSD results for both considered target false alarm rates. This corresponds to the trend demonstrated by the ROC curves in Figure 3. In the low SNRs C-EDR unsurprisingly performs worse than non-compressive Nyqist rate energy detector. However, one should bear in mind that the operating SNR range of C-DDR exactly corresponds to the SNR range generally required for signal recovery in sub-Nyquist sampling. It is also worth noting that C-DDR does not require setting any additional thresholds beyond the ones required for the execution of the

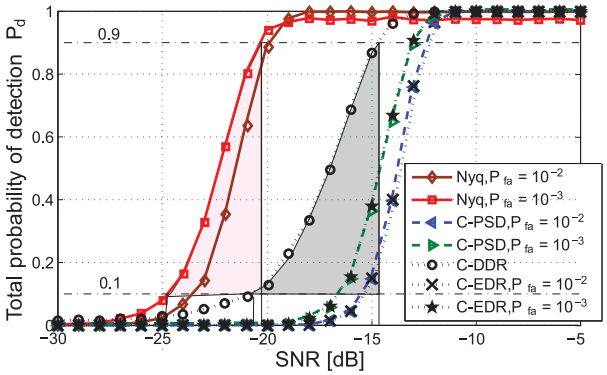

Fig. 4: Total probability of correct detection P_{d} vs. SNR for the case of a single signal sub-band that occupies exactly one spectral block

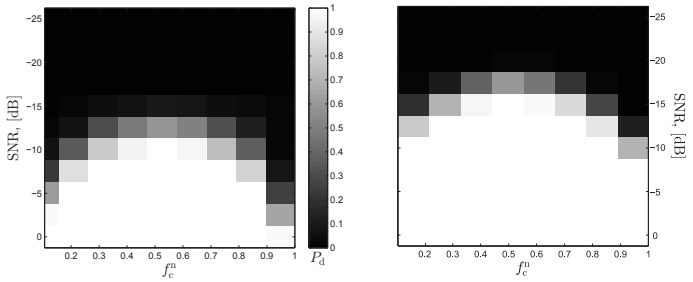

(a) C-DDR (b) Nyq, $P_{\mathrm{fa}} = 10^{-3}$

Fig. 5: Total probability of correct detection P_{d} vs. SNR vs. the position of the signal sub-band with regard to the center of a spectral block $f_{\mathrm{c}}^{\mathrm{n}} = f_{\mathrm{c}}/f_{\mathrm{s}} - \lfloor f_{\mathrm{c}}/f_{\mathrm{s}} \rfloor$ for the case of a single signal sub-band with $B/f_s \approx 0.92$

sparse recovery itself.

2) Single and multiple signal sub-bands: So far we have considered a single spectral block occupied by a single signal sub-band. In order to study how the position of the signal sub-band influences the detection performance, Figures 5(a) and (b) show the dependence of the P_{d} on the normalized signal sub-band central frequency $f_{\mathrm{c}}^{\mathrm{n}}$ and SNR for the proposed C-DDR and Nyquist reference detectors, respectively. In accordance to the discussion in Section III-B, for both detectors the best performance corresponds to the signal sub-bands with central frequencies that are odd multiples of $f_{\mathrm{s}}/2$, i.e. when the whole sub-band's energy is contained within exactly one spectral block. The performance however decays rapidly (by ≈ 5 dB for each 10% shift) with the increase of the deviation from this optimal position.

Finally, Figure 6 presents the results for the total posterior probability of correct detection versus SNR for the case when no restrictions were imposed on the positions of the active signal sub-bands, i.e., the f_{c_i}s were chosen uniformly at random from a finite set of W/LN values. Comparing the results for $K = 1$ in Fig. 6 with those from Fig. 4, one can see the influence of the mismatch between the chanellization parameters and distribution of the signal sub-bands in the overall performance deterioration: the shift of the curves to the higher SNRs and almost double stretching of the $[0.1, 0.9]$ interval.

V. Conclusion

In this work we proposed a compressive energy detector for blind coarse wideband spectrum sensing of sub-Nyquist

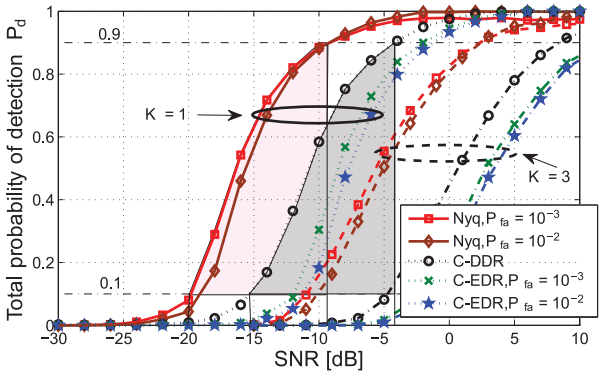

Fig. 6: Total probability of correct detection P_{d} vs. SNR for the case of no restrictions on the signal sub-band positions and the number of signal sub-bands $K = 1$ and $K = 3$

sampled sparse multiband signals. We analyzed how the mismatch between the signal and sampler parameters affect the resulting spectral accuracy and performed an extensive numerical performance study. Obtained results demonstrate that the proposed detector is superior to its direct counterpart while providing a comparative performance to the Nyquist sensing in the high SNR regime.

VI. Acknowledgments

This work was partly supported by the Deutsche Forschungsgemeinschaft (DFG) projects CoCoSa (grant MA 1184/26-1) and CLASS (grant MA 1184/23-1).

References

[1] Y. Bresler, "Spectrum-blind sampling and compressive sensing for continuous-index signals," in *Information Theory and Applications Workshop*. IEEE, 2008, pp. 547–554.

[2] M. Mishali and Y. C. Eldar, "Blind multiband signal reconstruction: Compressed sensing for analog signals," *Signal Processing, IEEE Trans. on*, vol. 57, no. 3, pp. 993–1009, 2009.

[3] M. Mishali and Y. Eldar, "From theory to practice: Sub-Nyquist sampling of sparse wideband analog signals," *Selected Topics in Signal Processing, IEEE Journal*, vol. 4, no. 2, pp. 375–391, 2010.

[4] Z. Tian and G. B. Giannakis, "Compressed sensing for wideband cognitive radios," in *Acoustics, Speech and Signal Processing. IEEE International Conference on*, vol. 4, 2007, pp. IV–1357.

[5] H. Sun, A. Nallanathan, C.-X. Wang, and Y. Chen, "Wideband spectrum sensing for cognitive radio networks: a survey," *Wireless Communications, IEEE*, vol. 20, no. 2, pp. 74–81, 2013.

[6] D. Arianandа and G. Leus, "Compressive wideband power spectrum estimation," *Signal Processing, IEEE Transactions on*, vol. 60, no. 9, pp. 4775–4789, Sept 2012.

[7] M. Rashidi, K. Haghighi, A. Panahi, and M. Viberg, "A NLLS based sub-nyquist rate spectrum sensing for wideband cognitive radio," in *New Frontiers in Dynamic Spectrum Access Networks, IEEE Symposium on*, 2011, pp. 545–551.

[8] D. Cohen and Y. C. Eldar, "Sub-nyquist sampling for power spectrum sensing in cognitive radios: A unified approach," *IEEE Transactions on Signal Processing*, vol. 62, pp. 3897–3910, 2014.

[9] M. A. Lexa, M. E. Davies, and J. S. Thompson, "Compressive and noncompressive power spectral density estimation from periodic nonuniform samples," *arXiv preprint arXiv:1110.2722*, 2011.

[10] M. Mishali and Y. C. Eldar, "Wideband spectrum sensing at sub-nyquist rates," *Signal Processing Magazine, IEEE*, vol. 28, pp. 102–135, 2011.

[11] Y. C. Eldar and G. Kutyniok, *Compressed sensing: theory and applications*. Cambridge University Press, 2012.

[12] J. Tropp, A. C. Gilbert *et al.*, "Signal recovery from random measurements via orthogonal matching pursuit," *Information Theory, IEEE Transactions on*, vol. 53, no. 12, pp. 4655–4666, 2007.